LETTER

doi:10.1038/nature25775

A suppression of differential rotation in Jupiter's deep interior

T. Guillot[1], Y. Miguel[1,2], B. Militzer[3], W. B. Hubbard[4], Y. Kaspi[5], E. Galanti[5], H. Cao[6,7], R. Helled[8], S. M. Wahl[3], L. Iess[9], W. M. Folkner[10], D. J. Stevenson[6], J. I. Lunine[11], D. R. Reese[12], A. Biekman[1], M. Parisi[10], D. Durante[9], J. E. P. Connerney[13], S. M. Levin[10] & S. J. Bolton[14]

Jupiter's atmosphere is rotating differentially, with zones and belts rotating at speeds that differ by up to 100 metres per second. Whether this is also true of the gas giant's interior has been unknown[1,2], limiting our ability to probe the structure and composition of the planet[3,4]. The discovery by the Juno spacecraft that Jupiter's gravity field is north–south asymmetric[5] and the determination of its non-zero odd gravitational harmonics J_3, J_5, J_7 and J_9 demonstrates that the observed zonal cloud flow must persist to a depth of about 3,000 kilometres from the cloud tops[6]. Here we report an analysis of Jupiter's even gravitational harmonics J_4, J_6, J_8 and J_{10} as observed by Juno[5] and compared to the predictions of interior models. We find that the deep interior of the planet rotates nearly as a rigid body, with differential rotation decreasing by at least an order of magnitude compared to the atmosphere. Moreover, we find that the atmospheric zonal flow extends to more than 2,000 kilometres and to less than 3,500 kilometres, making it fully consistent with the constraints obtained independently from the odd gravitational harmonics. This depth corresponds to the point at which the electric conductivity becomes large and magnetic drag should suppress differential rotation[7]. Given that electric conductivity is dependent on planetary mass, we expect the outer, differentially rotating region to be at least three times deeper in Saturn and to be shallower in massive giant planets and brown dwarfs.

Juno measurements of odd gravitational harmonics[5] constrain the maximum depth to which the observed atmospheric zonal flow persists[6]. These estimates, however, are based on the north–south asymmetries in the zonal flow, and cannot exclude the presence of a deeper north–south symmetric flow. Fortunately, further insights can be obtained by comparing the even gravitational harmonics obtained from interior models assuming rigid rotation with those expected for a differentially rotating planet. The harmonics from rigidly rotating interior models are highly correlated because they probe similar regions of the interior[8]. On the other hand, differential rotation similar to that observed in the cloud layer affects the different gravitational harmonics (moments) relatively evenly[9,10].

We derive an ensemble of interior models with Jupiter's mass and equatorial radius using both the CEPAM code[11] and by perturbing density profiles obtained by the Concentric MacLaurin Spheroid (CMS) code[12]. Our range of J_2 values is set by Juno's measurements and the maximum uncertainty due to the unknown interior differential rotation[10]. These models use different equations of state of hydrogen and helium[13,14], including a possible jump of up to 500 K in temperature in the helium phase-separation region, and the possibility (or not) of a dilute core[12]. The calculation of the gravitational harmonics is performed in two ways, with the CMS theory[15,16] directly or with a fourth-order theory of figures[17,18] combined with a direct integration of the reconstructed two-dimensional density structure using a Gauss–Legendre quadrature. A calibration of the values obtained from the theory of figures to the CMS values ensures an accurate estimate of the high-order J values (see Methods).

The offset between differential and rigid rotation for each harmonic i (with $2i = 2, 4, 6, 8, 10$), $\Delta J_{2i} = J_{2i}^{\mathrm{differential}} - J_{2i}^{\mathrm{rigid}}$, is calculated by assuming that the dynamical flows generate density perturbations that can be related through thermal wind balance[10,19]. We use a polynomial fit of degree m to the observed zonal winds[20] and an exponential decay in wind strength of e-folding depth H. We vary m between 2 and 30 and H between 0 km (rigid rotation) and 100,000 km (rotation on cylinders all the way to the centre of the planet), thus creating a wide range of possible interior flows. We use the Juno measurements[5] to calculate effective gravitational harmonics $J_{2i}^{\mathrm{eff}}(H, m) = J_{2i}^{\mathrm{Juno}} - \Delta J_{2i}(H, m)$. These are the values that must be matched by interior models assuming rigid rotation.

We compare the gravitational harmonics obtained from interior models to the effective gravitational harmonics in Fig. 1. Our interior models purposely cover a wide range of J_2 values, compatible with the Juno measurements and variable interior differential rotation, varying from a solution representing a very shallow region with differential rotation at the surface to one representing a deep region extending to the planet's centre (Fig. 1a). We also allow for a wide range of meridional profiles (m values), to allow for the possibility that the internal flows have less latitudinal variation than the cloud-level wind profile. We see that the extent of interior model solutions is noticeably smaller in J_4 versus J_6 and becomes a well defined linear relation in J_6 versus J_8, and J_8 versus J_{10}. On the other hand, differential rotation affects the J_{2i} values more uniformly as a function of the parameters H and m. The solutions are obtained by matching rigidly rotating interior models (black and grey dots) to the effective gravitational harmonics (coloured squares).

In the J_2 versus J_4 plane, any value of the effective gravitational harmonics can be matched by small adjustments of the assumed interior composition: no constraint on interior differential rotation is possible. In the J_4 versus J_6, J_6 versus J_8, and J_8 versus J_{10} planes, the same interior models are incompatible with most values of the effective gravitational harmonics. The corresponding values of H and m are therefore excluded. In the J_4 versus J_6 plane, the interior models cross the Juno point, providing only an upper limit on H. However, in the J_6 versus J_8, and J_8 versus J_{10} planes, the slight offset between the Juno point and the interior model area implies that a lower limit on H may be derived.

[1]Université Côte d'Azur, OCA, Lagrange CNRS, 06304 Nice, France. [2]Leiden Observatory, University of Leiden, Niels Bohrweg 2, 2333CA Leiden, The Netherlands. [3]University of California, Berkeley, California 94720, USA. [4]Lunar and Planetary Laboratory, University of Arizona, Tucson, Arizona 85721, USA. [5]Weizmann Institute of Science, Rehovot 76100, Israel. [6]California Institute of Technology, Pasadena, California 91125, USA. [7]Department of Earth and Planetary Sciences, Harvard University, Cambridge, Massachusetts 02138, USA. [8]University of Zurich, 8057 Zurich, Switzerland. [9]Sapienza Università di Roma, 00184 Rome, Italy. [10]Jet Propulsion Laboratory, California Institute of Technology, Pasadena, California 91109, USA. [11]Cornell University, Ithaca, New York 14853, USA. [12]LESIA, Observatoire de Paris, PSL Research University, CNRS, Sorbonne Universités, UPMC Université Paris 06, Université Paris Diderot, Sorbonne Paris Cité, 92195 Meudon, France. [13]NASA/GSFC, Greenbelt, Maryland, USA. [14]Southwest Research Institute, San Antonio, Texas, USA.

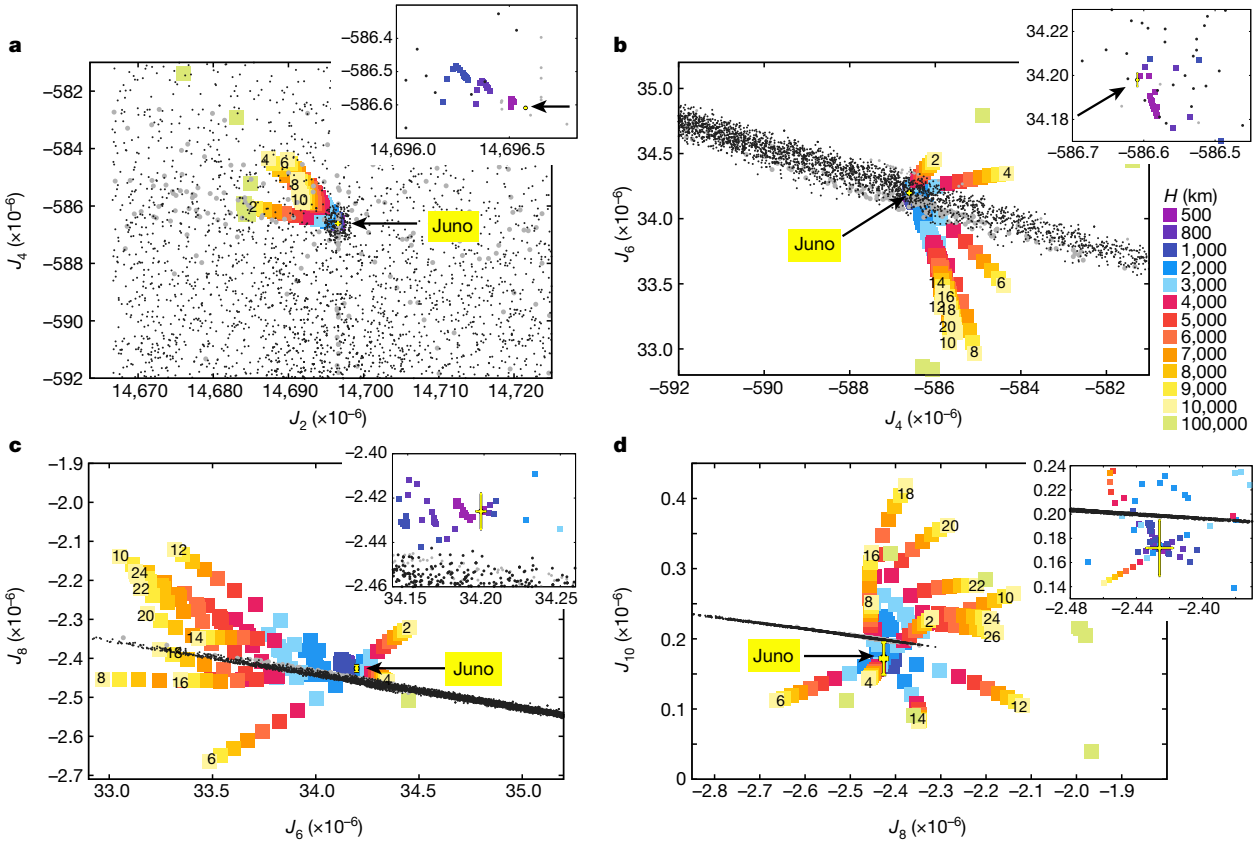

Figure 1 | Jupiter's gravitational harmonics J_2 to J_{10}. a, J_2 versus J_4. **b**, J_4 versus J_6. **c**, J_6 versus J_8. **d**, J_8 versus J_{10}. The points correspond to interior models of Jupiter calculated assuming rigid rotation using CEPAM[11] (black points) and CMS[12,15] (grey points). The coloured squares correspond to the values that must be matched by interior models in order to be considered successful solutions for observed zonal flows extending to various depths, from $H = 500$ km to $H = 100{,}000$ km, and by filtering the atmospheric flow (m from 2 to 30; see text)[10]. The numbers on the plots correspond to the value of m for $H = 10{,}000$ km. The Juno measurements and their 1σ error bars are shown in yellow. Because these are extremely small, arrows point to the corresponding points. Insets are close-ups around the Juno points for all four panels.

Mechanisms other than differential rotation cannot realistically explain that offset: in order to alter the relations between J_6, J_8 and J_{10}, they would need to strongly affect the interior density profile in the outer approximately 30% of the planet[8]. In this region, uncertainties in the H–He phase separation and related composition jumps are included in the interior model and constrained by the J_4 versus J_6 values. The other source of uncertainty is related to the condensation of water and silicates but is expected to affect J_4 by only about 10^{-7}, J_6 by 10^{-8} and J_8 by about 10^{-9}, that is, more than one order of magnitude less than required (see Methods).

To estimate possible values of the wind depth H (measured from the 1-bar level, approximately the cloud tops), we calculate the likelihood that an atmospheric model (accounting for the effect of differential rotation) combined with an interior model (accounting for the effect of interior structure) matches the observed even gravity coefficients. For a given value of H, we integrate the function $\exp[-(J_{2i}^{\mathrm{eff}}(H, m) - J_{2i}^{\mathrm{model}})^2/(2\sigma_{2i}^2)]/[(2\pi)^{1/2}\sigma_{2i}]$ over all models in our ensemble and all values of m. σ_{2i} encompasses the 1σ uncertainty of the Juno measurements as well as the variance in our ensemble of models. Figure 2 confirms the analysis of Fig. 1 that J_2 versus J_4 or J_4 versus J_6 alone cannot be used to constrain the wind depth H. The strongest constraints on H come from the J_6 versus J_8 and J_8 versus J_{10} planes because the weights of atmospheric contributions become large relative to those for the lower harmonics. When constraints from J_2 to J_{10} are combined, a strong peak emerges in the likelihood function in Fig. 2. Only values of H between 2,000 km and 3,500 km are compatible with the available data. This depth corresponds to the one at which the electrical conductivity[21] increases to a modest value (0.01–1 S m^{-1}) and

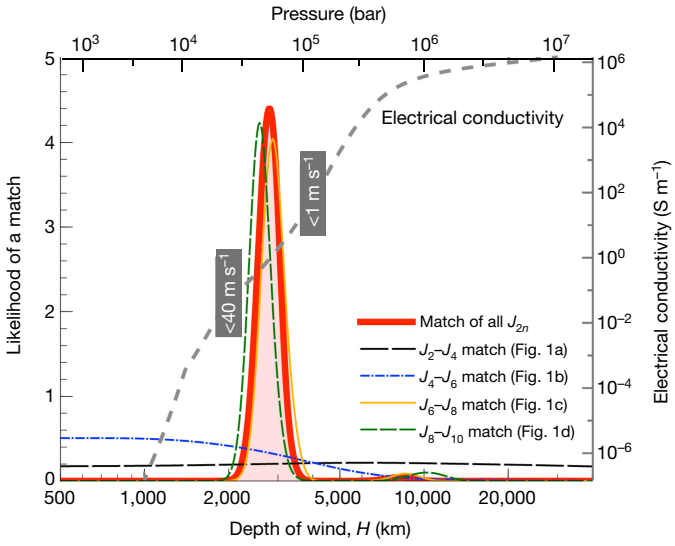

Figure 2 | Constraint on the depth H of Jupiter's zonal flow obtained from interior models and Juno's even gravitational harmonics. The lines correspond to Fig. 1a–d: J_2 versus J_4, J_4 versus J_6, J_6 versus J_8, and J_8 versus J_{10}. The profile of electrical conductivity in Jupiter's interior[21] is shown for comparison. Ohmic dissipation is expected to limit zonal flows[7] to less than 40 m s^{-1} at a depth of 2,000 km and to 1 m s^{-1} at 4,000 km. Only interior models with $-586.8 < J_4 \times 10^6 < -584.5$ (corresponding to the maximum range of J_4^{eff} values allowed by differential rotation) were included in the calculation.

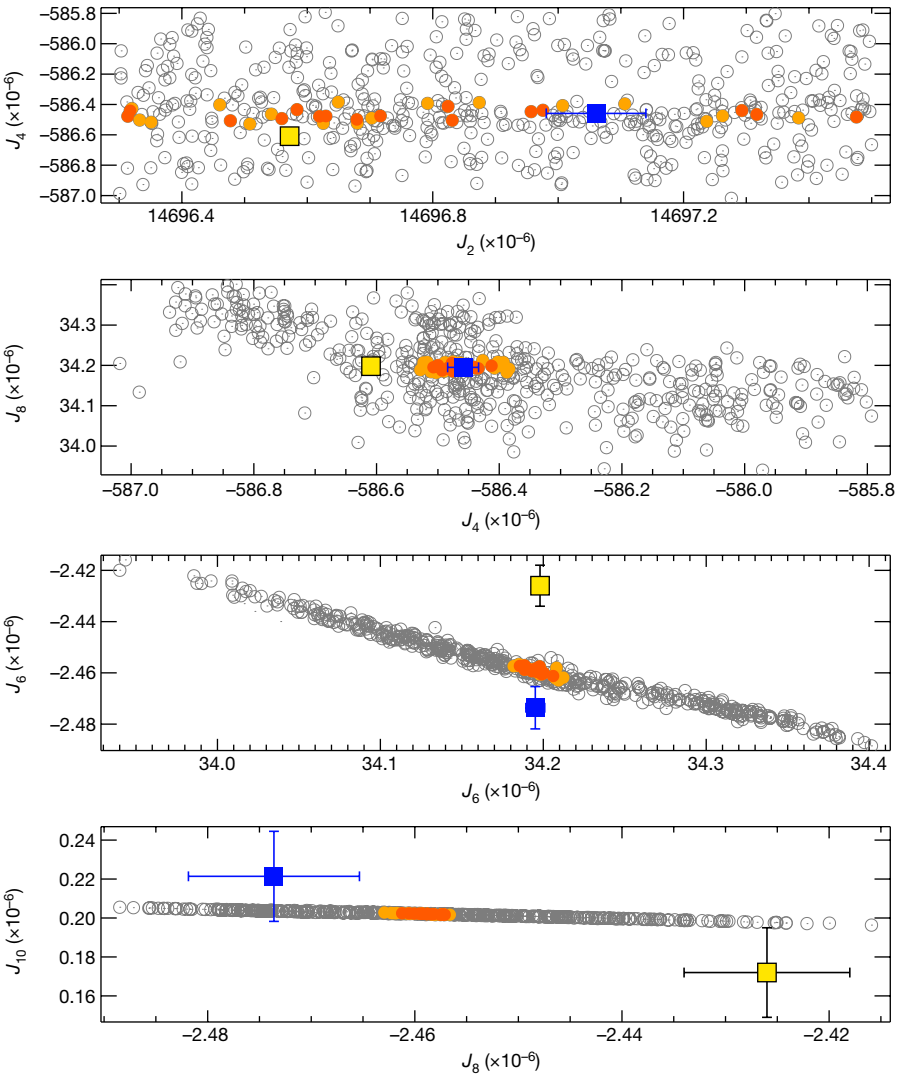

Figure 3 | Ensemble of interior models of Jupiter fitting the even gravitational harmonics J_2 to J_{10}. The Juno values are shown as yellow squares with 1σ error bars. The blue squares with 1σ error bars correspond to the effective gravitational harmonics obtained when accounting for the differential rotation derived from Jupiter's odd gravitational harmonics[6]. Interior models fitting all effective gravitational harmonics J_4 to J_{10} (blue squares) are highlighted in colour depending on whether they fit within 2σ (dark orange) or 3σ (light orange).

the Lorentz force associated with the zonal flow (magnetic drag) becomes comparable to the observed divergence of the Reynolds stress in the cloud layers[7,22,23]. Indeed, energy budget considerations of the ohmic dissipation being smaller than the observed luminosity predict a penetration depth between about 2,000 km and 2,800 km below the cloud tops of Jupiter[7,24].

The results obtained in Figs 1 and 2 are based on a simple law (an exponential decay of the atmospheric zonal flow) that was obtained independently of Juno's measurements[10]. In Fig. 3 we show that the more elaborate differential-rotation law that is fitted to Jupiter's odd gravitational harmonics[6] is consistent with the interior models, confirming that the symmetric and asymmetric parts of the observed zonal flow extend to a similar depth. The solutions matching the observations generally cover an extensive parameter space (see Extended Data Table 1). One salient feature is that these solutions are characterized by an increase of the heavy-element abundance in the deeper interior, either where hydrogen becomes metallic or deeper in a dilute core, confirming the results obtained after Juno's first two orbits[12].

Furthermore, by adopting the differential rotation law for the upper 3,000 km of Jupiter's atmosphere, we can provide approximate constraints on the rotation of the deeper parts of the planet. To do so, we assume that the deeper interior rotates on cylinders all the way to the centre and adopt a scaled version of the ΔJ_{2i} relations from Fig. 1. We calculate the likelihood of such a model with unknown deep differential rotation v between zero and the observed atmospheric rotation of about 100 m s^{-1}, using the same approach as for Fig. 2 (see Methods). The results are shown in Extended Data Fig. 2. Only an upper limit may be derived on v: beneath the first 3,000-km-deep layer, deep differential rotation must be limited to amplitudes at least an order of magnitude smaller than the observed atmospheric ones.

The observed winds thus penetrate deep in the atmosphere all the way to the levels at which the conductivity and the resulting magnetic drag become large enough to force fluid motions into rigid-body rotation[23,24]. In gaseous planets, electrical conductivity strongly increases with pressure, which is itself a strong function of the planetary mass. In Saturn, one must go three times deeper than in Jupiter to reach the same conductivity[7,21]. Saturn has a similar intrinsic luminosity but a magnetic field that is an order of magnitude smaller than Jupiter's[25]. We hence expect Saturn's outer, differentially rotating region to extend to at least 9,000 km, which should leave a strong imprint on its gravity field. Conversely, massive giant exoplanets and brown dwarfs should have shallower differentially rotating, outer envelopes[26].

Online Content Methods, along with any additional Extended Data display items and Source Data, are available in the online version of the paper; references unique to these sections appear only in the online paper.

Received 19 September 2017; accepted 17 January 2018.

1. Busse, H. F. A simple model of convection in the Jovian atmosphere. *Icarus* **29,** 255–260 (1976).
2. Vasavada, A. R. & Showman, A. P. Jovian atmospheric dynamics: an update after Galileo and Cassini. *Rep. Prog. Phys.* **68,** 1935–1996 (2005).
3. Hubbard, W. B. Effects of differential rotation on the gravitational figures of Jupiter and Saturn. *Icarus* **52,** 509–515 (1982).
4. Guillot, T., Gautier, D. & Hubbard, W. B. New constraints on the composition of Jupiter from Galileo measurements and interior models. *Icarus* **130,** 534–539 (1997).
5. Iess, L. *et al.* Measurement of Jupiter's asymmetric gravity field. *Nature* **555,** https://doi.org/10.1038/nature25776 (2018).
6. Kaspi, Y. *et al.* Jupiter's atmospheric jet streams extend thousands of kilometres deep. *Nature* **555,** https://doi.org/10.1038/nature25793 (2018).
7. Cao, H. & Stevenson, D. J. Zonal flow magnetic field interaction in the semi-conducting region of giant planets. *Icarus* **296,** 59–72 (2017).
8. Guillot, T. The interiors of giant planets: models and outstanding questions. *Annu. Rev. Earth Planet. Sci.* **33,** 493–530 (2005).
9. Hubbard, W. B. Gravitational signature of Jupiter's deep zonal flows. *Icarus* **137,** 357–359 (1999).
10. Kaspi, Y. *et al.* The effect of differential rotation on Jupiter's low-degree even gravity moments. *Geophys. Res. Lett.* **44,** 5960–5968 (2017).
11. Miguel, Y., Guillot, T. & Fayon, L. Jupiter internal structure: the effect of different equations of state. *Astron. Astrophys.* **596,** A114 (2016).
12. Wahl, S. M. *et al.* Comparing Jupiter interior structure models to Juno gravity measurements and the role of an expanded core. *Geophys. Res. Lett.* **44,** 4649–4659 (2017).
13. Militzer, B. & Hubbard, W. B. Ab initio equation of state for hydrogen-helium mixtures with recalibration of the giant-planet mass-radius relation. *Astrophys. J.* **774,** 148 (2013).
14. Becker, A. *et al.* Ab initio equations of state for hydrogen (H-REOS.3) and helium (He-REOS.3) and their implications for the interior of brown dwarfs. *Astrophys. J. Suppl. Ser.* **215,** 21 (2014).
15. Hubbard, W. B. Concentric Maclaurin spheroid models of rotating liquid planets. *Astrophys. J.* **768,** 43 (2013).
16. Wisdom, J. & Hubbard, W. B. Differential rotation in Jupiter: a comparison of methods. *Icarus* **267,** 315–322 (2016).
17. Zharkov, V. N. & Trubitsyn, V. P. *Physics Of Planetary Interiors* (Astronomy and Astrophysics Series, Pachart, 1978)
18. Nettelmann, N. Low- and high-order gravitational harmonics of rigidly rotating Jupiter. *Astron. Astrophys.* **606,** A139 (2017).
19. Kaspi, Y., Showman, A. P., Hubbard, W. B., Aharonson, O. & Helled, R. Atmospheric confinement of jet streams on Uranus and Neptune. *Nature* **497,** 344–347 (2013).
20. Ingersoll, A. P. *et al.* in *Jupiter. The Planet, Satellites And Magnetosphere* (eds Bagenal, F., Dowling, T. E. & McKinnon, W. B.) *Cambridge Planetary Science* Vol. 1, 105–128 (Cambridge Univ. Press, 2004).
21. French, M. *et al.* Ab initio simulations for material properties along the Jupiter adiabat. *Astrophys. J. Suppl. Ser.* **202,** 5 (2012).
22. Salyk, C., Ingersoll, A. P., Lorre, J., Vasavada, A. & Del Genio, A. D. Interaction between eddies and mean flow in Jupiter's atmosphere: analysis of Cassini imaging data. *Icarus* **185,** 430–442 (2006).
23. Schneider, T. & Liu, J. Formation of jets and equatorial superrotation on Jupiter. *J. Atmos. Sci.* **66,** 579–601 (2009)
24. Liu, J., Goldreich, P. M. & Stevenson, D. J. Constraints on deep-seated zonal winds inside Jupiter and Saturn. *Icarus* **196,** 653–664 (2008).
25. Connerney, J. E. P. in *Planets and Satellites* (eds Schubert, G. & Spohn, T.) *Treatise in Geophysics* Vol. 10.06, 195–237 (Elsevier, 2015).
26. Showman, A. P. & Guillot, T. Atmospheric circulation and tides of "51 Pegasus b-like" planets. *Astron. Astrophys.* **385,** 166–180 (2002).

Acknowledgements This research was carried out at the Observatoire de la Côte d'Azur under the sponsorship of the Centre National d'Etudes Spatiales; at the Jet Propulsion Laboratory, California Institute of Technology, under a contract with NASA; by the Southwest Research Institute under contract with NASA; and at the Weizmann Institute of Science under contract with the Israeli Space Agency. Computations were performed on the 'Mesocentre SIGAMM' machine, hosted by the Observatoire de la Côte d'Azur.

Author Contributions T.G., Y.M. and B.M. ran interior models of Jupiter and carried out the analysis. W.B.H. and A.B. compared gravitational harmonics obtained by different methods. E.G. and Y.K. calculated the offset introduced by differential rotation. H.C., R.H., D.J.S. and J.I.L. provided theoretical support. S.M.W. provided additional interior models of Jupiter. D.R.R. provided a routine to calculate high-order gravitational harmonics efficiently. W.M.F., M.P. and D.D. carried out the analysis of the Juno gravity data. J.E.P.C., S.M.L. and S.J.B. supervised the planning, execution and definition of the Juno gravity experiment.

Author Information Reprints and permissions information is available at www.nature.com/reprints. The authors declare no competing financial interests. Readers are welcome to comment on the online version of the paper. Publisher's note: Springer Nature remains neutral with regard to jurisdictional claims in published maps and institutional affiliations. Correspondence and requests for materials should be addressed to T.G. (tristan.guillot@oca.eu).

Reviewer Information *Nature* thanks J. Fortney and N. Nettelmann for their contribution to the peer review of this work.

METHODS

Calculation of interior models. The internal structure of Jupiter is calculated using the equations of hydrostatic equilibrium, energy transport, energy and mass conservation, which are solved with the interior structure code CEPAM[27]. These models are constructed to fit observational constrains such as Jupiter's radius and gravitational harmonics.

We adopt a four-layer structure for the interior models: (1) a helium-poor upper envelope in which hydrogen is in molecular form, (2) a helium-rich, metallic-hydrogen lower envelope, (3) a dilute core which consists of helium-rich metallic hydrogen with an increase of the heavy-element content and (4) a central dense core of ices and rocks. Because convection tends to homogenize large fractions of the envelope[28], we expect that regions (1) and (2) should be largely convective and homogeneous. However, the presence of a phase separation[29] of helium in metallic hydrogen at about 1 Mbar may create a barrier to convection[30–32] and thus yield an increase in both helium and heavy-element abundances. The dilute core region may be inhomogeneous and an extension of the core itself[33,34].

The determination of Jupiter's internal structure still rests on the accuracy of the equations of state[11,35,36]. For H and He we use two of the most recently published equations of state calculated from *ab initio* simulations: MH13[13] and REOS3[14]. For REOS3-H and REOS3-He, the pure hydrogen and pure helium equation-of-state tables, respectively, we calculate the entropy with a dedicated procedure[11]. MH13 was produced for a fixed mixture of H and He. To allow different concentrations of H and He in the different layers we extract from MH13 the table for H and since MH13 does not cover the entire pressure range in Jupiter's interior we merge the extracted table with the Saumon–Chabrier–van Horn equation of state[11,36]. The heavy elements are assumed to be composed of rocks and ices[37].

Since we attempt to calculate the largest possible ensemble of realistic interior models we allow for the possibility of either efficient convection or double-diffusive convection in the helium phase-separation region by including a possible jump in temperature in that region[30–32,35,38]. Uncertainties in the location and characteristics of the helium phase-separation zone are considered by varying the limit[29] between region (1) and region (2) between 0.8 Mbar and 3 Mbar. Uncertainty about the presence of the dilute-core region (3) is included by performing some of the calculations either without this region (three-layer models) or with region (3) and including three variable parameters: the location of the transition, its smoothness and the heavy-element fraction in the transition region.

To obtain this large ensemble of possible interior models, for each set of imposed parameters, we obtain the mass fraction of ices in region (1) and the core mass that best fits the observed equatorial radius of the Jupiter[39], 71,492 ± 4 km and the gravitational harmonic J_2 following an optimization procedure[40]. We do not attempt to fit the other gravitational harmonics and we allow for a large range of values for J_2 between 0.014665 and 0.014725 in order to probe the ensemble of possible solutions, from rigidly rotating solutions to differential rotation extending all the way to the planetary centre.

Extended Data Table 1 summarizes the parameters used in the models. Their values are drawn either from a Gaussian distribution when they are constrained observationally or from a uniform distribution when we do not have sufficient a priori knowledge of their value. More than 200,000 interior models were calculated.

We calculate models in which the amount of water and rocks is suppressed at temperatures below 200 K and 3,000 K, respectively, in order to mimic the condensation of these species. The changes to J_4 (about 10^{-7}), to J_6 (about 10^{-8}) and to J_8 (about 10^{-9}) are found to be too small to affect the results.

We also use an alternative method in which we perturb the density profiles for Jupiter[9] and calculate their gravitational harmonics using CMS. We introduce between 1 and 4 density jumps at random pressures. The magnitudes of the density changes are also chosen randomly between −5% and +5% to represent possible compositional deviations or equation-of-state deviations that are not yet understood. These thus represent a wide ensemble of models—some of them unphysical (for example, because of a decrease in density with increasing pressure). Nevertheless, the inferred ensemble of gravitational harmonics (grey points in Fig. 1) overlaps very closely with that obtained using full interior structure models (black points), suggesting that the results, in terms of the gravitational moments of a rigidly rotating Jupiter, are robust.

Calculation of gravitational harmonics. The calculation of the gravitational harmonics is performed as follows: for the CMS model and their perturbations we use the CMS approach[15,16]. For the CEPAM models, we use the faster theory of figures to fourth order[17,18] to obtain a bi-dimensional interior density profile $\rho(\zeta, \theta)$ where ζ is the (dimensionless) mean radius and θ the colatitude. We then calculate the gravitational harmonics J_l as:

$$J_l = -\frac{1}{MR^l}\int_0^1\int_0^{2\pi}\int_0^{\pi} r^l \rho(\zeta,\theta) P_\ell(\cos\theta) r^2 |r_\zeta| \sin\theta \mathrm{d}\theta \mathrm{d}\Phi \mathrm{d}\zeta$$

where M and R are the planetary mass and equatorial radius, respectively, r_ζ is the partial derivative of r with respect to ζ, and $P_l(\cos\theta)$ is the Legendre polynomial of degree l. We use a Gauss–Legendre quadrature in the horizontal direction θ and finite differences in the radial direction ζ.

Extended Data Table 2 shows a comparison of solutions obtained from this method and from two other approaches. First, we use CEPAM on an $n = 1$ polytropic equation of state and compare the solution to that calculated using an extremely accurate method[16]. The results are in good agreement, with offsets being at most 1.5×10^{-7}. These offsets are a natural consequence of the theory of figures expansion[17,18]. We then compare more realistic Jupiter models calculated with CEPAM and with the CMS method. The offsets for high-order harmonics are remarkably similar to the ones obtained for the polytropic model. The offsets for J_2 are comparatively more important and are believed to be due to discretization errors[16]. These imply a small error on the core mass and the mass of heavy elements in the planet by an amount that is negligible in regard to the other uncertainties[18]. By comparing the solutions obtained with two slightly different models having the same J_2 value with CEPAM and CMS, respectively (line REOS1a-1b in Extended Data Table 2), we can see that the offset in J_2 has a small effect on J_4 and an even smaller one on higher-order harmonics.

Using these results, we adopt the following offsets $\delta J_4 = 0.11 \times 10^{-6}$, $\delta J_6 = -0.057 \times 10^{-6}$, $\delta J_8 = 0.166 \times 10^{-6}$, $\delta J_{10} = -0.029 \times 10^{-6}$. Although we expect this offset to change slightly as a function of the parameters used, the level of precision obtained is sufficient to derive constraints on the internal differential rotation. This is shown in Extended Data Fig. 1, which compares calculations performed with the different approaches.

Constraints on deep differential rotation. To derive constraints on the amount of differential rotation underneath the 'atmospheric' layer, we proceed as follows: First we imagine that we can divide the interior into a differentially rotating outer shell tied to the atmospheric zonal wind and a deeper layer with a smaller amount of differential rotation (with characteristic zonal velocity v) all the way to the centre of Jupiter. Given that the rotation of the outer shell is constrained by the odd harmonics, we wish to find the possible values of v. We therefore need to associate effective gravitational harmonics J_{2i}^{obs} with each value of v.

We do so by adding Juno's value, the offset derived from the latitude-dependent flow profile that best fits Juno's odd harmonics, and a deeper component that is obtained from the purely cylindrical component for $H = 100{,}000$ km (see Fig. 1)[10]:

$$J_{2i}^{\mathrm{obs}} = J_{2i}^{\mathrm{Juno}} - \delta J_{2i}^{\mathrm{oddfit}} - \frac{v}{100\ \mathrm{m\,s^{-1}}} \delta J_{2i}^{H=100{,}000\ \mathrm{km}}(m)$$

where we assume that the value of δJ_{2i} obtained for the atmospheric zonal flows ($v \approx 100\ \mathrm{m\,s^{-1}}$) may be scaled linearly for any characteristic velocity v.

We then calculate the likelihood of these models as a function of v with the same approach as for Fig. 2, including all gravitational harmonics J_4 to J_{10}. The results are plotted in Extended Data Fig. 2. For our preferred model, we obtain a strong upper limit at $10\ \mathrm{m\,s^{-1}}$ with a preference for smaller values of v. For $v < 6\ \mathrm{m\,s^{-1}}$ the best interior models are found to lie within two standard deviations of all effective gravitational harmonics. For comparison, a model with a thin weather layer ($H = 0$) and differential rotation on cylinders to the centre with velocity v is also found to favour small values of $v < 10\ \mathrm{m\,s^{-1}}$ but is incompatible with Juno's gravitational harmonics.

Code availability. The CEPAM code is available for download at https://svn.oca.eu/codes/CEPAM/trunk.

Data availability. Data sharing is not applicable to this article as no datasets were generated during the current study.

27. Guillot, T. & Morel, P. CEPAM: a code for modeling the interiors of giant planets. *Astron. Astrophys.* **109,** 109–123 (1995).
28. Vazan, A., Helled, R., Podolak, M. & Kovetz, A. The evolution and internal structure of Jupiter and Saturn with compositional gradients. *Astrophys. J.* **829,** 118 (2016).
29. Morales, M. A., Hamel, S., Caspersen, K. & Schwegler, E. Hydrogen-helium demixing from first principles: from diamond anvil cells to planetary interiors. *Phys. Rev. B* **87,** 174105 (2013).
30. Stevenson, D. J. & Salpeter, E. E. The dynamics and helium distribution in hydrogen-helium fluid planets. *Astrophys. J. Suppl. Ser.* **35,** 239–261 (1977).
31. Nettelmann, N., Fortney, J. J., Moore, K. & Mankovich, C. An exploration of double diffusive convection in Jupiter as a result of hydrogen-helium phase separation. *Mon. Not. R. Astron. Soc.* **447,** 3422–3441 (2015).
32. Mankovich, C., Fortney, J. J. & Moore, K. L. Bayesian evolution models for Jupiter with helium rain and double-diffusive convection. *Astrophys. J.* **832,** 113 (2016)
33. Stevenson, D. J. Cosmochemistry and structure of the giant planets and their satellites. *Icarus* **62,** 4–15 (1985).
34. Helled, R. & Stevenson, D. The fuzziness of giant planets' cores. *Astrophys. J.* **840,** L4 (2017).

35. Hubbard, W. B. & Militzer, B. A preliminary Jupiter model. *Astrophys. J.* **820,** 80 (2016).
36. Saumon, D., Chabrier, G. & van Horn, H. M. An equation of state for low-mass stars and giant planets. *Astrophys. J. Suppl. Ser.* **99,** 713–741 (1995).
37. Saumon, D. & Guillot, T. Shock compression of deuterium and the interiors of Jupiter and Saturn. *Astrophys. J.* **609,** 1170–1180 (2004).
38. Leconte, J. & Chabrier, G. A new vision of giant planet interiors: impact of double diffusive convection. *Astron. Astrophys.* **540,** A20 (2012).
39. Lindal, G. F. The atmosphere of Neptune—an analysis of radio occultation data acquired with Voyager 2. *Astron. J.* **103,** 967–982 (1992).
40. Guillot, T. A comparison of the interiors of Jupiter and Saturn. *Planet. Space Sci.* **47,** 1183–1200 (1999).
41. Seiff, A. *et al.* Thermal structure of Jupiter's atmosphere near the edge of a 5-micron hot spot in the north equatorial belt. *J. Geophys. Res.* **103,** 22857–22889 (1998).
42. Serenelli, A. M. & Basu, S. Determining the initial helium abundance of the Sun. *Astrophys. J.* **719,** 865–872 (2010).
43. von Zahn, U., Hunten, D. M. & Lehmacher, G. Helium in Jupiter's atmosphere: results from the Galileo probe helium interferometer experiment. *J. Geophys. Res.* **103,** 22815–22829 (1998).

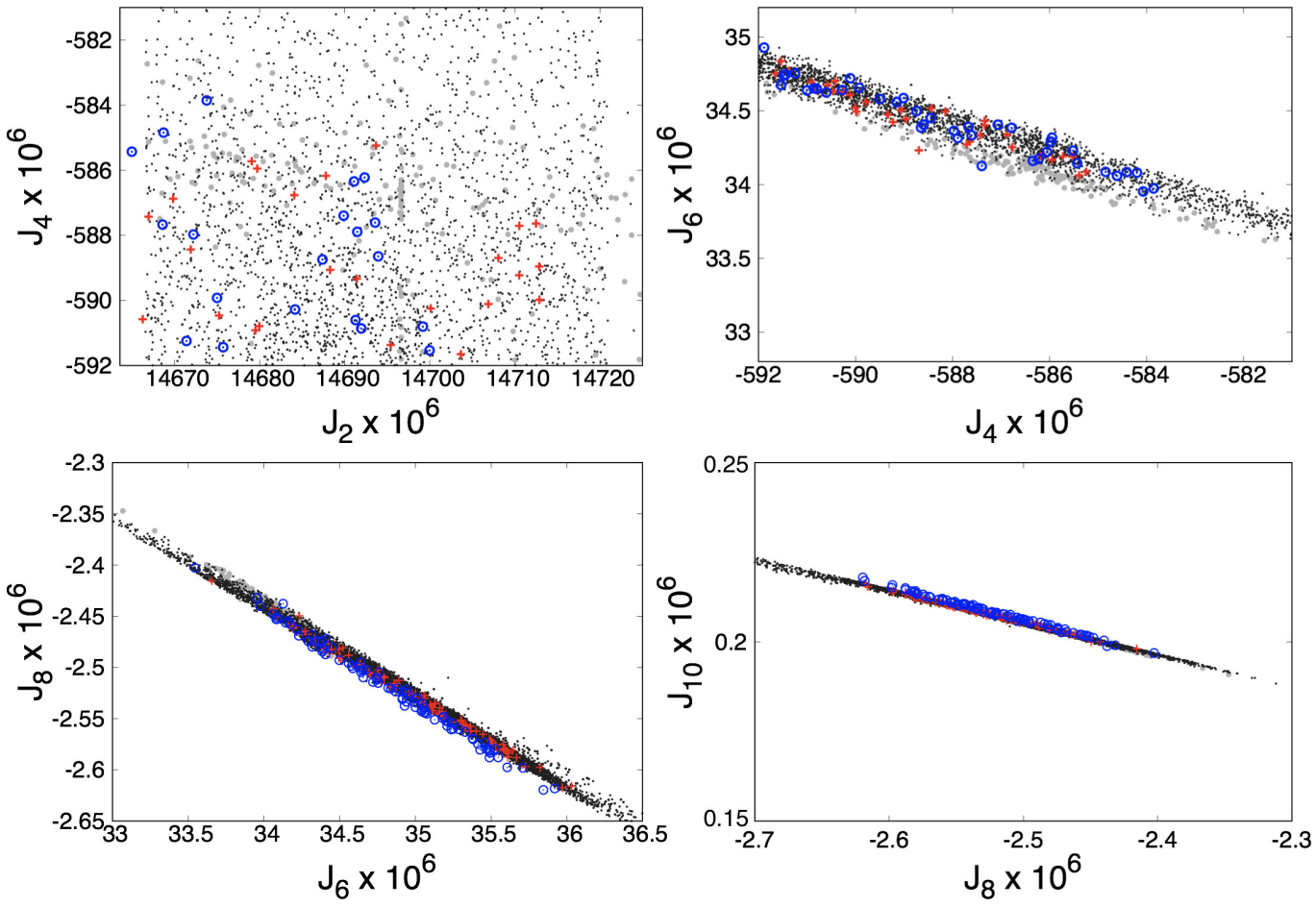

Extended Data Figure 1 | Validation of the calculation of gravitational harmonics with the CEPAM method. The four panels provide a comparison of gravitational harmonics J_2 to J_{10} calculated with various methods: CEPAM models with 241 radial layers (black points), CMS models with 800 layers (grey points), CEPAM models with 1,041 layers (red crosses), and CMS calculations for the CEPAM models with 1,041 layers (blue circles).

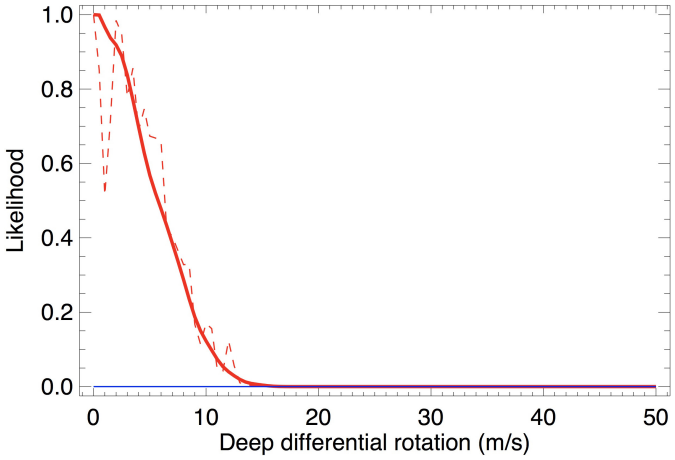

Extended Data Figure 2 | Constraint on the characteristic amplitude of deep differential rotation in Jupiter. The red curves show the likelihood of models (y axis) in which to the differentially rotating outer region constrained by Juno's odd harmonics[6] we add a deeper cylindrical flow of amplitude v (x axis). The dashed red curve uses 1σ error bars. The solid red curve considers an extended ensemble of possibilities for the outer flow[6] with solutions up to 3σ. In both cases, the model favours $v < 6\,\mathrm{m\,s^{-1}}$. The blue curve shows the same model but without the added outer layer. That model also favours low-amplitude winds but is found to be 4×10^4 times less likely than the model including the differentially rotating outer region.

Extended Data Table 1 | Parameters used for the calculation of interior models

Parameter	Description	Type	Mean	σ or ΔX
T_{1bar}	1 bar temperature, from Voyager and Galileo measurements [39,41]	Gaussian	165K	4K
$Y_{proto}/(X_{proto}+Y_{proto})$	Protosolar helium mixing ratio obtained from solar models [42]	Gaussian	0.277	0.006
$Y_{atm}/(X_{atm}+Y_{atm})$	Helium mixing ratio in Jupiter's atmosphere as measured by the Galileo probe [43]	Gaussian	0.238	0.005
P_{He}	Characteristic pressure of the helium phase separation region [29,32]	Uniform	1.9 Mbar	1.1 Mbar
ΔT_{He}	Temperature increase over the helium phase separation region [12]	Uniform	0	500 K
$L_{dilcore}$	Presence of the diluted core region	Binary	0/1	
$P_{dilcore}$	Pressure of the diluted core region	Uniform	21.5 Mbar	18.5 Mbar
$\Delta \log P_{dilcore}$	Smoothness of the diluted core transition	Uniform	0.0255	0.0245
$\Delta Z_{dilcore}$	Mass mixing ratio increase in the diluted core region	Uniform	0.2	0.2
$Z_{ices}^{(1)}$	Mass mixing ratio of ices in region (1)	Fitted		
$Z_{rocks}^{(1)}$	Mass mixing ratio of rocks in region (1)	Uniform	0.025	0.025
ΔZ_{ices}	Jump in the mass mixing ratio of ices from region (1) to region (2)	Uniform	0.075	0.075
ΔZ_{rocks}	Jump in the mass mixing ratio of rocks from region (1) to region (2)	Uniform	0.075	0.075
M_{core}	Mass of the central dense core	Fitted		

Data are from refs 12, 29, 32, 39, 41–43.

Extended Data Table 2 | Comparison of model gravitational harmonics

Model	Method	$J_2\times10^6$	$J_4\times10^6$	$J_6\times10^6$	$J_8\times10^6$	$J_{10}\times10^6$	$J_{12}\times10^6$
Polytrope	CEP	13988.65	-531.8675	30.06605	-1.98248	0.14772	-0.01201
	WH16	13988.51	-531.8281	30.11832	-2.13212	0.17407	-0.01568
	CEP-WH16	0.14	-0.0394	-0.05227	0.14964	-0.02635	0.00367
REOS1a	CEP	14696.72	-587.8227	34.22564	-2.29778	0.17296	-0.01413
	CMS	14690.66	-587.3989	34.26170	-2.46234	0.20218	-0.01821
	CEP-CMS	6.06	-0.4238	-0.03606	0.16456	-0.02922	0.00408
REOS1b	CEP	14702.78	-588.1331	34.24635	-2.29937	0.17309	-0.01414
	CMS	14696.72	-587.7090	34.28245	-2.46399	0.20232	-0.01822
	CEP-CMS	6.06	-0.4240	-0.03610	0.16462	-0.02923	0.00408
REOS1a-1b	CEP-CMS	-0.00	-0.1136	-0.05681	0.16621	-0.02936	0.00409
MH13	CEP	14695.97	-590.2377	34.46524	-2.31752	0.17465	-0.01428
	CMS	14690.96	-589.9033	34.51000	-2.48443	0.20422	-0.01841
	CEP-CMS	5.01	-0.3343	-0.04476	0.16691	-0.02957	0.00413